Model Predictive Control-Based Direct Torque Control for Matrix Converter-Fed Induction Motor with Reduced Torque Ripple

Hanbing Dan, Peng Zeng, Wenjing Xiong, Meng Wen, Mei Su, and Marco Rivera

***Abstract*—To reduce the torque ripple in motors resulting from the use of conventional direct torque control (DTC), a model predictive control (MPC)-based DTC strategy for a direct matrix converter-fed induction motor is proposed in this paper. Two new look-up tables are proposed, these are derived on the basis of the control of the electromagnetic torque and stator flux using all the feasible voltage vectors and their associated switching states. Finite control set model predictive control (FCS-MPC) has then been adopted to select the optimal switching state that minimizes the cost function related to the electromagnetic torque. Finally, the experimental results are shown to verify the reduced torque ripple performance of the proposed MPC-based DTC method.**

***Index Terms*—Direct torque control, finite control set model predictive control, induction motor, matrix converter.**

I. INTRODUCTION

MATRIX converter (MC) has attracted a lot of attention due to its inherent advantages, such as bi-directional energy flow, controllable input power factor, the potential for high power density, and the lack of bulky dc-link capacitors [1-4]. Previous studies are mainly concentrated on the modulation and the switching pattern of the MC [5]-[6]. High-performance speed control for MC-fed induction motors (IM) has received less attention. The direct torque control (DTC) method for MC-fed IM was first proposed by Casadei [7] and was then experimentally verified [8]. Nevertheless, variable frequency operation, torque ripple and flux ripple have been identified as the main drawbacks [9]. Several methods based on constant switching frequency [10] and switching tables [11] imposition in DTC have been employed to overcome these problems. In [10], an improved direct torque control-space vector method was proposed, which used the space vector method and a flux dead-beat algorithm to decrease the torque ripple and obtain unity input power factor. In [11], an improved DTC method is proposed, which is based on twelve 30° sectors of both voltage and flux vectors for MC-fed IM. A new lookup table was developed and the optimal switching vector was selected for control of the torque with minimized variations of the stator flux within the hysteresis band. As a result, a lower torque ripple was obtained compared to the conventional DTC method, however, the required look-up table is complex.

The FCS-MPC has been developed and applied to the control of power converter and motor drives because of its advantages such as fast dynamic response, easy inclusion of nonlinearities and constraints of the system, and the flexibility to include other system requirements in the controller [12]-[16]. In [17], an improved model predictive torque control is proposed for a 2-level voltage source inverter-fed induction motor drive, which reduces the control complexity and torque ripple. In [18], a weighting factor optimization method for reducing the torque ripple of inductions machine fed by an indirect matrix converter is presented. In [19], a predictive current control method for an IM based on the MC was proposed, which uses MPC to control the stator current and hence achieves the control of torque and flux of the IM. All 27 valid switching states are utilized in the cost function, which is time-consuming. In [20], MPC is used to control the electromagnetic torque and the stator flux. Nevertheless, it still considers all 27 switching states, so the problem of time-consuming calculations is left unsolved. Several methods have been proposed to reduce the calculation effort for the MC with the FCS-MPC method [21]-[22].

To reduce the torque ripple caused by conventional DTC strategy, an improved MPC-based DTC strategy for a direct matrix converter-fed (DMC-fed) IM is proposed in this paper. Consistent with the theory of direct torque control, the proposed method achieves the desired control effect through the direct control of electromagnetic torque and stator flux.

Two look-up tables are proposed in order to fully utilize the available switching states. Nine switching states are preselected according to the two look-up tables, saving considerable processor time in the calculations. Then, MPC is used to select the optimal switching state, which will be used in the next control period. Some principle of the proposed MPC-based

Manuscript received March 02, 2021; revised April 12, 2021; accepted April 28, 2021. date of publication June 25, 2021; date of current version June 18, 2021.

This work was supported in part by the Hunan Provincial Key Laboratory of Power Electronics Equipment and Grid under Grant 2018TP1001, in part by the National Natural Science Foundation of China under Grant 61903382, 51807206, 61933011, in part by the Major Project of Changzhutan Self-Dependent Innovation Demonstration Area under Grant 2018XK2002, in part by the Natural Science Foundation of Hunan Province, China under Grant 2020JJ5722 and 2020JJ5753. *(Corresponding author: Wenjing Xiong).*

Hanbing Dan, Peng Zeng, Wenjing Xiong, Mei Su are with the Hunan Provincial Key Laboratory of Power Electronics Equipment and Gird, School of Automation, Central South University, Changsha, 410083 China (email: daniel698@sina.cn, 194611007@csu.edu.cn, csu.xiong@163.com, sumeicsu@mail.csu.edu.cn).

Meng Wen is with the Yunnan Mobile Communication Company Limited, Yunnan, 678000 China (e-mail: wenmeng90@163.com).

M. Rivera is with the Department of Electrical Engineering, Universidad de Talca, Curico, PB, 3341717 Chile (e-mail: marcoesteban@gmail.com).

Digital Object Identifier 10.30941/CESTEMS.2021.00012

TABLE I
SPACE VECTORS OF DMC

Categories	Switching states	A B C	v_{om}	α_o	i_{im}	β_i
I	+1	a b b	2/3 v_{iab}	0	$2/\sqrt{3}i_{oa}$	-π/6
I	-1	b a a	-2/3 v_{iab}	0	$-2/\sqrt{3}i_{oa}$	-π/6
I	+2	b c c	2/3 v_{ibc}	0	$2/\sqrt{3}i_{oa}$	π/2
I	-2	c b b	-2/3 v_{ibc}	0	$-2/\sqrt{3}i_{oa}$	π/2
I	+3	c a a	2/3 v_{ica}	0	$2/\sqrt{3}i_{oa}$	7π/6
I	-3	a c c	-2/3 v_{ica}	0	$-2/\sqrt{3}i_{oa}$	7π/6
I	+4	b a b	2/3 v_{iab}	2π/3	$2/\sqrt{3}i_{ob}$	-π/6
I	-4	a b a	-2/3 v_{iab}	2π/3	$-2/\sqrt{3}i_{ob}$	-π/6
I	+5	c b c	2/3 v_{ibc}	2π/3	$2/\sqrt{3}i_{ob}$	π/2
I	-5	b c b	-2/3 v_{ibc}	2π/3	$-2/\sqrt{3}i_{ob}$	π/2
I	+6	a c a	2/3 v_{ica}	2π/3	$2/\sqrt{3}i_{ob}$	7π/6
I	-6	c a c	-2/3 v_{ica}	2π/3	$-2/\sqrt{3}i_{ob}$	7π/6
I	+7	b b a	2/3 v_{iab}	4π/3	$2/\sqrt{3}i_{oc}$	-π/6
I	-7	a a b	-2/3 v_{iab}	4π/3	$-2/\sqrt{3}i_{oc}$	-π/6
I	+8	c c b	2/3 v_{ibc}	4π/3	$2/\sqrt{3}i_{oc}$	π/2
I	-8	b b c	-2/3 v_{ibc}	4π/3	$-2/\sqrt{3}i_{oc}$	π/2
I	+9	a a c	2/3 v_{ica}	4π/3	$2/\sqrt{3}i_{oc}$	7π/6
I	-9	c c a	-2/3 v_{ica}	4π/3	$-2/\sqrt{3}i_{oc}$	7π/6
II	0	a a a	0	—	0	—
II	0	b b b	0	—	0	—
II	0	c c c	0	—	0	—
III	—	a b c	v_{im}	α_i	i_{om}	β_o
III	—	a c b	$-v_{im}$	$-\alpha_i$	i_{om}	$-\beta_o$
III	—	b a c	$-v_{im}$	$-\alpha_i$ +4π/3	i_{om}	$-\beta_o+2\pi/3$
III	—	b c a	v_{im}	α_i +4π/3	i_{om}	$\beta_o+2\pi/3$
III	—	c a b	v_{im}	α_i +2π/3	i_{om}	$\beta_o+4\pi/3$
III	—	c b a	$-v_{im}$	$-\alpha_i$ +2π/3	i_{om}	$-\beta_o+4\pi/3$

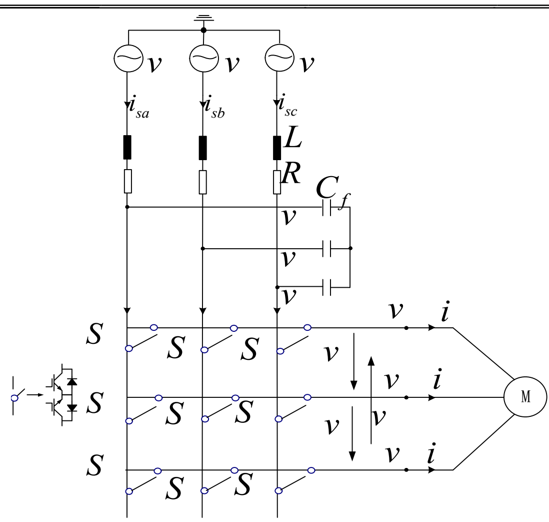

Fig. 1. Topology of direct matrix converter

DTC for MC-fed IM in this paper is described in [23], more principle details and experimental results are added in this paper.

This paper has been structured as follows: Section II introduces the topology of a direct matrix converter. Section III introduces the conventional direct torque control for the MC-fed induction motor and analyses the main reason that causes high torque ripple. Section IV proposes an MPC-based DTC for DMC-fed IM. Finally, Section V verifies the feasibility and correction of the proposed MPC-based DTC method. Section VI concludes the findings. Section VII discusses the performance of the proposed method with the performance of the conventional DTC method and conventional FCS-MPC method.

II. TOPOLOGY OF THE DIRECT MATRIX CONVERTER

As Fig. 1 shows, there are nine bidirectional switches present in the DMC, each of which is here to make sure that bi-directional energy flow works. Connected between the grid and the converter, the input filter aims to eliminate high harmonic distortion in the grid current. According to the topology of the DMC, the mathematical model of input and output of the DMC can be written as:

$$\begin{bmatrix} v_{oa} \\ v_{ob} \\ v_{oc} \end{bmatrix} = \begin{bmatrix} S_{Aa} & S_{Ab} & S_{Ac} \\ S_{Ba} & S_{Bb} & S_{Bc} \\ S_{Ca} & S_{Cb} & S_{Cc} \end{bmatrix} \begin{bmatrix} v_{ia} \\ v_{ib} \\ v_{ic} \end{bmatrix} \tag{1}$$

$$\begin{bmatrix} i_{ia} \\ i_{ib} \\ i_{ic} \end{bmatrix} = \begin{bmatrix} S_{Aa} & S_{Ab} & S_{Ac} \\ S_{Ba} & S_{Bb} & S_{Bc} \\ S_{Ca} & S_{Cb} & S_{Cc} \end{bmatrix}^T \begin{bmatrix} i_{oa} \\ i_{ob} \\ i_{oc} \end{bmatrix} \tag{2}$$

$$S = \begin{bmatrix} S_{Aa} & S_{Ab} & S_{Ac} \\ S_{Ba} & S_{Bb} & S_{Bc} \\ S_{Ca} & S_{Cb} & S_{Cc} \end{bmatrix} \tag{3}$$

where v_{ol} ($l \in \{a,b,c\}$), v_{ij} ($j \in \{a,b,c\}$) represents the output voltage and filter capacitor voltage, respectively. i_{ol} , i_{ij} represents the output current and input current. S_{Xy} ($X \in \{A,B,C\}$, $y \in \{a,b,c\}$) represents the switching states of nine bidirectional switches, which satisfy the following equation:

$$S_{Xy} = \begin{cases} 1 & S_{Xy} \text{ is on} \\ 0 & S_{Xy} \text{ is off} \end{cases} \tag{4}$$

Considering the following restrictions of the DMC:
(1) No open circuit for the output of DMC;
(2) No short circuit for the input of DMC.
Thus, the following equation should be satisfied:

$$\begin{cases} S_{Aa}+S_{Ab}+S_{Ac}=1 \\ S_{Ba}+S_{Bb}+S_{Bc}=1 \\ S_{Ca}+S_{Cb}+S_{Cc}=1 \end{cases} \tag{5}$$

There are 27 valid switching states of DMC, and each switching state along with their output voltage and input current are listed in Table I. All switching states can be divided into three categories:

Category I: each switching state can generate space vectors with fixed direction and variable amplitude, named as "active vectors".

Category II: the amplitude of the space vector is zero with variable direction, which is called "zero vectors".

Category III: the direction of the space vectors generated by the switching states under this category are variable whereas the amplitude is fixed, and the vectors are titled "rotating vectors".

Since each active vector (category I) has a fixed direction, the active voltage vector can fall into six directions in the α-β plane, as shown in Fig. 2a.

The output voltage vector $\boldsymbol{v}_o$ and input current vector $\boldsymbol{i}_i$ can be expressed as:

$$\boldsymbol{v}_o = \frac{2}{3}(v_{oa} + v_{ob}e^{j(2\pi/3)} + v_{oc}e^{j(4\pi/3)}) = v_{om}e^{j\alpha_o} \tag{6}$$

$$\boldsymbol{i}_i = \frac{2}{3}(i_{ia} + i_{ib}e^{j(2\pi/3)} + i_{ic}e^{j(4\pi/3)}) = i_{im}e^{j\beta_i} \tag{7}$$

where v_{om} , i_{im} represent the amplitude of $\boldsymbol{v}_o$ and, $\boldsymbol{i}_i$, respectively. α_o and β_i represent the angle of $\boldsymbol{v}_o$ and $\boldsymbol{i}_i$, respectively. The source voltage vector $\boldsymbol{v}_{sa}, \boldsymbol{v}_{sb}, \boldsymbol{v}_{sc}$, source current vector $\boldsymbol{i}_{sa}, \boldsymbol{i}_{sb}, \boldsymbol{i}_{sc}$ and output current vector $\boldsymbol{i}_{oa}, \boldsymbol{i}_{ob}, \boldsymbol{i}_{oc}$ can be obtained by the same method.

According to the mathematical model of the input filter, the state-space description is obtained as follow:

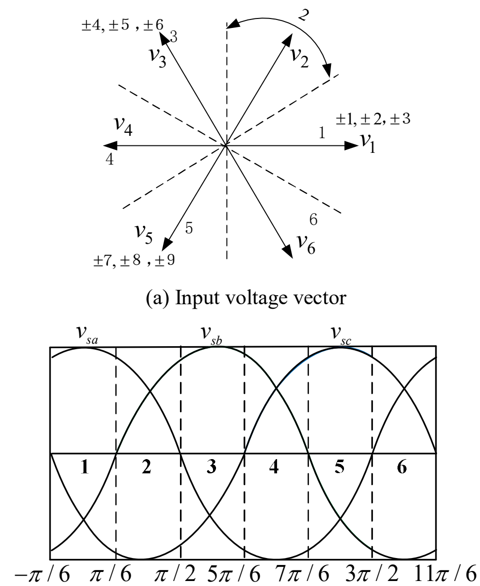

(b) Voltage sector division

Fig. 2. Input voltage vector division in conventional DTC method.

$$\begin{bmatrix} \dfrac{d\boldsymbol{v}_i}{dt} \\ \dfrac{d\boldsymbol{i}_s}{dt} \end{bmatrix} = N\begin{bmatrix} \boldsymbol{v}_i \\ \boldsymbol{i}_s \end{bmatrix} + M\begin{bmatrix} \boldsymbol{v}_s \\ \boldsymbol{i}_i \end{bmatrix} \tag{8}$$

where N and M are the matrixes which can be expressed as follows:

$$N = \begin{bmatrix} 0 & 1/C_f \\ -1/L_f & -R_i/L_f \end{bmatrix}, M = \begin{bmatrix} 0 & -1/C_f \\ 1/L_f & 0 \end{bmatrix} \tag{9}$$

where C_f is the filter capacitor, L_f is the filter inductance, R_i is the passive damping resistor.

Among those vectors (v_1~v_6), the α-β axis can be split up into six sectors S_n (n=1…6), the range of each sector should satisfy the following equation:

$$(2n-3)\pi/6 \le s_n \le (2n\text{-}1)\pi/6 \tag{10}$$

Considering the sector where the input voltage is located, every two switching states can generate voltage vectors of the same direction. For example, as Fig. 2(b) shows, assuming that the input voltage located in sector 1, the direction of v_{sac} is not fixed, $v_{sac}> 0$, $v_{sab} > 0$, so the switching state +1 and -3 can generate an output voltage whose direction is the same as that of v_1. Therefore, the relationship between the voltage vector and the switching states in different voltage sectors under the DTC method is explained in Table II.

III. CONVENTIONAL DIRECT TORQUE CONTROL FOR INDUCTION MOTOR

Assuming that the following conditions are satisfied:
(1) Three-phase winding of induction motor is completely symmetrical in the structure;
(2) The magnetic saturation and the core loss of induction motor are ignored;
(3) The effect on parameters of IM can be ignored when the temperature and frequency are variable.

The mathematical model of IM can be obtained as follow:

TABLE II
RELATIONSHIP BETWEEN VOLTAGE VECTORS AND SWITCHING STATES IN DIFFERENT VOLTAGE SECTORS UNDER DTC METHOD

Voltage vector	Voltage Sector					
	1	2	3	4	5	6
$\vec{v_1}$	-3, +1	+2, -3	-1, +2	+3, -1	-2, +3	+1, -2
$\vec{v_2}$	+9, -7	-8, +9	+7, -8	-9, +7	+8, -9	-7, +8
$\vec{v_3}$	-6, +4	+5, -6	-4, +5	+6, -4	-5, +6	+4, -5
$\vec{v_4}$	+3, -1	-2, +3	+1, -2	-3, +1	+2, -3	-1, +2
$\vec{v_5}$	-9, +7	+8, -9	-7, +8	+9, -7	-8, +9	+7, -8
$\vec{v_6}$	+6, ,-4	-5, +6	+4, -5	-6, +4	+5, -6	-4, +5

$$\boldsymbol{v}_o = R_s \boldsymbol{i}_o + \frac{d\boldsymbol{\varphi}_s}{dt} \tag{11}$$

$$\boldsymbol{\varphi}_s = L_s \boldsymbol{i}_o + L_m \boldsymbol{i}_r \tag{12}$$

$$\boldsymbol{\varphi}_r = L_r \boldsymbol{i}_r + L_m \boldsymbol{i}_o \tag{13}$$

$$T_e = \frac{3}{2} p(\boldsymbol{\varphi}_s \times \boldsymbol{i}_o) \tag{14}$$

where $\boldsymbol{v}_o$, $\boldsymbol{i}_o$, $\boldsymbol{i}_r$, $\boldsymbol{\varphi}_s$, $\boldsymbol{\varphi}_r$, T_e are the stator voltage vector, stator current vector, rotor current vector, stator flux vector, rotor flux vector and electromagnetic torque, respectively. R_s, L_s, L_r, L_m, p are the stator resistance, stator inductance, rotor inductance, mutual inductance and the pole pairs of IM, respectively.

Thus, according to (11)-(14), the following equation can be obtained when the voltage of stator resistance is ignored:

$$\Delta\varphi_s = \boldsymbol{v}_o \Delta t \tag{15}$$

$$T_e = \frac{3}{2} p \frac{L_m}{\sigma L_s L_r} |\varphi_s||\varphi_r| \sin\gamma \tag{16}$$

$$\sigma = 1 - \frac{L_m^2}{L_s L_r} \tag{17}$$

where $\Delta\varphi_s$ shows the change of stator flux during the time Δt, while γ represents the angle between rotor flux and stator flux. The main idea of a DTC based on DMC is to regard DMC and IM as a whole, using the space vector analysis method to select the appropriate switching state, thereby achieving direct control of the stator flux and the electromagnetic torque. As seen in Fig. 3, it is assumed that φ_s lies in sector 1 and $\varphi_s < \varphi_s^*$, $T_e < T_e^*$, the selection of voltage vector v_2 can increase φ_s and T_e. Therefore, the flux and electromagnetic torque errors are decreased. The optimal voltage vector can be selected by the stator flux vector and the relationship between the actual and reference values of stator flux and electromagnetic torque, which is summarized in Table III.

However, there are still some shortages of conventional DTC such as relatively high torque ripple. For example, from Fig. 3, if $\theta \in (-\pi/6, 0)$, voltage vector v_1 should also be regarded as a candidate which can reduce errors between φ_s and φ_s^*, but result in a large torque ripple. In order to decrease the torque ripples of the DTC, an MPC-based DTC strategy for a DMC-fed IM is proposed.

TABLE III
VOLTAGE SELECTION TABLE OF THE CONVENTIONAL DTC

Comparison of actual value and reference value		Stator flux sector 1	2	3	4	5	6
$\varphi_s < \varphi_s^*$	$T_e < T_e^*$	$\vec{v_2}$	$\vec{v_3}$	$\vec{v_4}$	$\vec{v_5}$	$\vec{v_6}$	$\vec{v_1}$
	$T_e \geq T_e^*$	$\vec{v_6}$	$\vec{v_1}$	$\vec{v_2}$	$\vec{v_3}$	$\vec{v_4}$	$\vec{v_5}$
$\varphi_s > \varphi_s^*$	$T_e < T_e^*$	$\vec{v_3}$	$\vec{v_4}$	$\vec{v_5}$	$\vec{v_6}$	$\vec{v_1}$	$\vec{v_2}$
	$T_e \geq T_e^*$	$\vec{v_5}$	$\vec{v_6}$	$\vec{v_1}$	$\vec{v_2}$	$\vec{v_3}$	$\vec{v_4}$

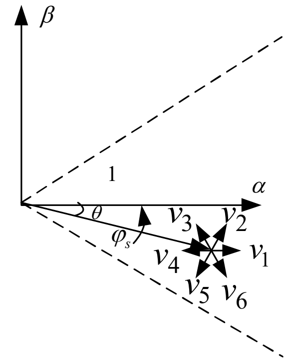

Fig. 3. Effect of voltage vector on stator flux

IV. PROPOSED MPC-BASED DTC STRATEGY FOR A DMC-FED IM

Fig. 4 illustrates the control diagram of the MPC-based DTC strategy. The main idea of the MPC-based DTC strategy for a DMC-fed IM is to establish an alternative voltage vector table that contains all available voltage vectors and switching states, as shown in Table IV and Table V, and use model predictive control to choose the optimal switching state to act on the DMC in the next control period.

TABLE IV
RELATIONSHIP BETWEEN VOLTAGE VECTORS AND THE NEW VOLTAGE SECTORS UNDER MPC-BASED DTC METHOD

Voltage vector	New voltage sector					
	1	2	3	4	5	6
$\vec{v_1}$	+1,+2,-3	-1,+2,-3	-1,+2,+3	-1,-2,+3	+1,-2,+3	+1,-2,-3
$\vec{v_2}$	-7,-8,+9	+7,-8,+9	+7,-8,-9	+7,+8,-9	-7,+8,-9	-7,+8,+9
$\vec{v_3}$	+4,+5,-6	-4,+5,-6	-4,+5,+6	-4,-5,+6	+4,-5,+6	+4,-5,-6
$\vec{v_4}$	-1,-2,+3	+1,-2,+3	+1,-2,-3	+1,+2,-3	-1,+2,-3	-1,+2,+3
$\vec{v_5}$	+7,+8,-9	-7,+8,-9	-7,+8,+9	-7,-8,+9	+7,-8,+9	+7,-8,-9
$\vec{v_6}$	-4,-5,+6	+4,-5,+6	+4,-5,-6	+4,+5,-6	-4,+5,-6	-4,+5,+6

A. Determination of alternative switch table

The torque ripple of a DTC is mainly caused by two reasons:
(1) Losses of alternative voltage vector.
(2) Division of the sector leading to the uncertainty in the direction of the output voltage of DMC.

In order to solve the above problems, a new voltage selection table of DTC and a new definition of voltage sector are obtained as Table IV and Fig. 5. In Table IV, all voltage vectors that can reduce the errors between the references and corresponding actual values are included, and in Fig. 5, the range of the new voltage sector is redefined as follows:

$$(n-1)\pi/3 \leq s_n' \leq n\pi/3 \tag{18}$$

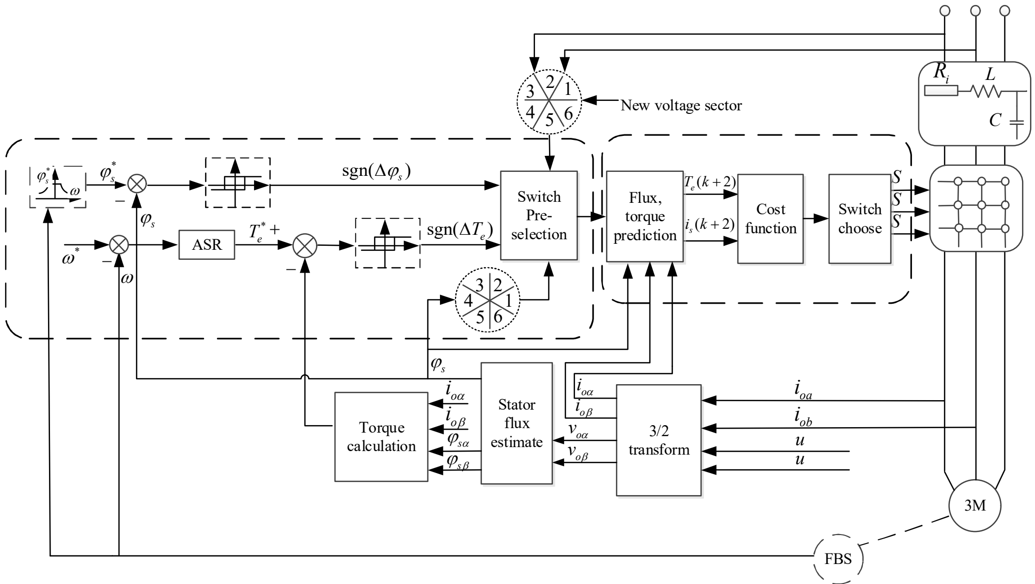

Fig. 4. Control diagram of the proposed method

As shown in Fig. 5, in sector 1, $v_{sa} > v_{sb} > v_{sc}$, switching state +2 can produce the voltage vector whose direction is the same as v_1, therefore, Table II can be expanded into Table V. Hence, according to Table IV and Table V, in each control period, there are nine possible switching states (containing zero voltage vectors) that can be used to reduce errors between the reference and actual value since there is only one switching state needed for the following control period, the MPC is here to predict and choose the optimal switching state among those nine switching states.

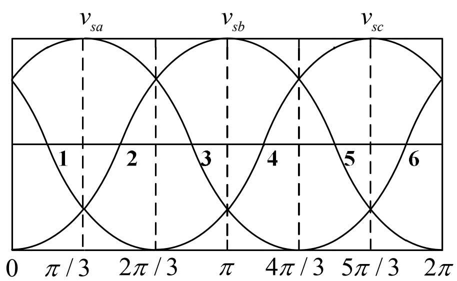

Fig. 5 New Input Voltage sector division under the proposed MPC

TABLE V
VOLTAGE SELECTION TABLE OF PROPOSED MPC-BASED DTC METHOD

Comparison of actual value and reference value		Stator flux sector 1	2	3	4	5	6
$\varphi_s < \varphi_s^*$	$T_e < T_e^*$	$\vec{v}_1,\vec{v}_2$	$\vec{v}_2,\vec{v}_3$	$\vec{v}_3,\vec{v}_4$	$\vec{v}_4,\vec{v}_5$	$\vec{v}_5,\vec{v}_6$	$\vec{v}_6,\vec{v}_1$
	$T_e \ge T_e^*$	$\vec{v}_6,\vec{v}_1$	$\vec{v}_1,\vec{v}_2$	$\vec{v}_2,\vec{v}_3$	$\vec{v}_3,\vec{v}_4$	$\vec{v}_4,\vec{v}_5$	$\vec{v}_5,\vec{v}_6$
$\varphi_s > \varphi_s^*$	$T_e < T_e^*$	$\vec{v}_3,\vec{v}_4$	$\vec{v}_4,\vec{v}_5$	$\vec{v}_5,\vec{v}_6$	$\vec{v}_6,\vec{v}_1$	$\vec{v}_1,\vec{v}_2$	$\vec{v}_2,\vec{v}_3$
	$T_e \ge T_e^*$	$\vec{v}_4,\vec{v}_5$	$\vec{v}_5,\vec{v}_6$	$\vec{v}_6,\vec{v}_1$	$\vec{v}_1,\vec{v}_2$	$\vec{v}_2,\vec{v}_3$	$\vec{v}_3,\vec{v}_4$

B. Model predictive control

To obtain the optimal switching state in each control period, model predictive control plays a crucial role in the MPC-based DTC. In MPC, the Euler formula shown in (19) is used to discretize the control objectives.

$$\frac{dx}{dt} \approx \frac{x(k+1)-x(k)}{T_s} \tag{19}$$

where T_s represents the sample period, k represents the control period. Therefore, the value of $\varphi_s(k+1)$ and $T_e(k+1)$ under all feasible switching states can be considered as the predictive value of stator flux and electromagnetic torque, and is evaluated in the cost function.

$$\varphi_s(k+1) = T_s v_o(k) - T_s R_s i_o + \varphi_s(k) \tag{20}$$

where

$$\varphi_s(k) = L_s i_o(k) + L_m i_r(k) \tag{21}$$

and $T_e(k+1)$ could be obtained as follows:

$$T_e(k+1) = \frac{3}{2} p\left[\varphi_{s\alpha}(k+1) i_{o\beta}(k+1) - \varphi_{s\beta}(k+1) i_{o\alpha}(k+1)\right] \tag{22}$$

where $\varphi_{s\alpha}(k+1)$, $\varphi_{s\beta}(k+1)$ are the prediction of stator flux in *(k+1)*th sample period under the two-phase stationary coordinate system(α-β axis), and can be obtained as follows:

$$\begin{bmatrix} \varphi_\alpha \\ \varphi_\beta \end{bmatrix} = \frac{2}{3}\begin{bmatrix} 1 & -\frac{1}{2} & -\frac{1}{2} \\ 0 & \frac{\sqrt{3}}{2} & -\frac{\sqrt{3}}{2} \end{bmatrix}\begin{bmatrix} \varphi_{sa} \\ \varphi_{sb} \\ \varphi_{sc} \end{bmatrix} \tag{23}$$

Besides, the stator current $i_{o\alpha}(k+1)$, $i_{o\beta}(k+1)$, can be obtained in the same way.

To achieve the grid current control, the prediction of reactive power is also considered as a part of the cost function. The equation of the prediction of reactive power is as follows:

$$Q(k+1) = u_{s\beta}(k+1) i_{s\alpha}(k+1) - u_{s\alpha}(k+1) i_{s\alpha}(k+1) \tag{24}$$

where *Q(k+1)* represents the input reactive power prediction, $u_{s\alpha,\beta}(k+1)$ and $i_{s\alpha,\beta}(k+1)$ represent the predicted value of grid voltage and grid current under α-β axis, and can be obtained by discretizing (8):

$$\begin{bmatrix} v_i(k+1) \\ i_s(k+1) \end{bmatrix} = D \begin{bmatrix} v_i(k) \\ i_s(k) \end{bmatrix} + E \begin{bmatrix} v_s(k) \\ i_i(k) \end{bmatrix} \tag{25}$$

$$v_s(k+1) \approx v_s(k) \tag{26}$$

where

$$D = e^{NT_s} \tag{27}$$

$$E = N^{-1}(D-I)M \tag{28}$$

Considering the huge computation of the MPC method, as well as the delay caused by the processor, the value of *(k+2)*th sample time is usually adopted as the predictive value. And to obtain the predictive values of *(k+2)*th sample time, the same method is used as that of *(k+1)*th sample time. To control stator flux and electromagnetic torque, and achieve sinusoidal source current, the square of the error between $\varphi_s(k+2)$, $T_e(k+2)$, $Q(k+2)$, and their references are chosen as a part of the cost function. Therefore, the cost function can be expressed as (29).

$$\begin{aligned} f = \lambda_T[T_e(k+2)-T_e^*]^2 + \lambda_1[\varphi_s(k+2)-\varphi_s^*]^2 + \\ \lambda_2[Q(k+2)-Q^*]^2 \end{aligned} \tag{29}$$

where λ_T,,λ_1, λ_2 are weighing factors. The values of these parameters will determine the priority of corresponding control variables [24-25].

Then, the optimal switching state of the next control period can be obtained by choosing the switching state minimizing the cost function *f*.

Hence, the overall control flow of the MPC-based DTC strategy for a DMC-fed IM can be summarized as follows:

Step1: Sampling of currents, voltages and speed.

Step2: Using the closed-loop flux observer [26]-[27] based on voltage and current model to observe $\varphi_s(k)$, and calculate $T_e(k)$.

Step3: $\varphi_s(k+1)$, $T_e(k+1)$, $Q(k+1)$ are the predictive values of (k+1)*th* sample time, which can be derived according to the load motor model and input filter model.

Step4: By comparing the reference value of stator flux and electromagnetic torque with their actual value, choosing 9 switching states that can reduce the error between actual and references joint Table IV and V.

Step5: Prediction of $\varphi_s(k+2)$, $T_e(k+2)$, $Q(k+2)$ with the 9 switching states selected in step4 according to the load motor model and input filter model.

Step6: Choosing the optimal switching state.

V. Experiment Results

This section conducts an experiment test under a low-voltage model, which can be seen in Fig. 6. The experimental setup is based on a 1.3kW induction motor, with a DMC driving the IM, whose parameters are shown in Table VI. The source line-to-line voltage is 200V (root mean square). The sample time is 70μs for the proposed MPC-based DTC method and conventional DTC method. The execution time of the proposed algorithm in DSP is 44μs. The weighing factors λ_T, λ_1, λ_2 are 10, 48, and 0.003, respectively. The switches of the MC are implemented by the insulated gate bipolar transistor (IGBT, FF200R12KT3_E). To get the signals of the optimal switching state, a digital signal processor (DSP, TMS320F28335) and the field-programmable gate array (FPGA, EP2C8J144C8N) are used. In order to obtain an equal load torque, a resistor (R=30Ω) is connected into each phase of the permanent magnet synchronous motor's stator, whose rotor is coaxial with the rotor of an IM.

TABLE VI
EXPERIMENTAL PARAMETERS

Parameters	Values
Number of pole pairs	2
Stator resistor (Ω)	6.4
Stator inductance (mH)	0.575
Rotor resistor (Ω)	4.8
Rated power (kW)	1.3
Rated speed (r/min)	1500
Source line to line voltage (V)	200
Input filter inductance (mH)	0.6
Input filter capacitance (μF)	66
Sample time(μs)	70

Fig. 7a and 7b show the waveform of the stator voltage, stator current of the IM and grid current by using the conventional DTC method and the proposed method, respectively, in which the load torque is set at 0 (N.m), the stator flux reference equals to 0.8 (Wb) and the speed reference is 600 (r/min). The input and output current are nearly sinusoidal in both methods.

Fig. 8a is the performance of rotor speed and stator flux amplitude of the conventional DTC method under the same condition of Fig. 7. As seen in Fig. 8a, the rotor speed tracks the reference with a deviation of 1.6% approximately, and the stator flux amplitude tracks references more accurately.

Fig. 8b shows the performance of the proposed MPC-based DTC method. As shown in Fig. 8b, the waveform of rotor speed, as the same with the conventional method, and the rotor speed tracks reference with a deviation of 1.6% approximately. Fig. 8b also shows the stator flux amplitude ripple of the MPC-based DTC method, which is smaller than the stator flux amplitude ripple under the conventional DTC.

The comparison of electromagnetic torque between the conventional DTC and MPC-based DTC method is shown in Fig. 8c. The red line is the electromagnetic torque under the conventional DTC method, and the blue line represents the electromagnetic torque under the MPC-based DTC method.

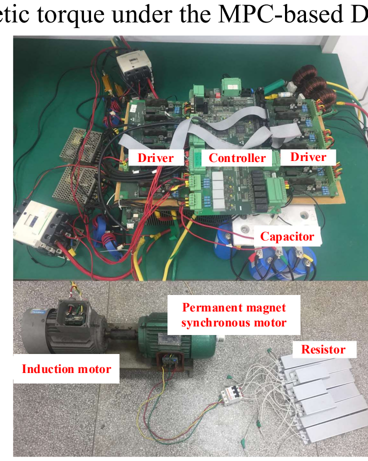

Fig. 6. Experimental setup

Though the load torque is set at 0, considering the factors such as friction that will affect the rotor rotation, the electromagnetic torque with both methods can only be maintained nearly to zero. However, compared to the conventional DTC method, the torque ripple under the proposed method is considerably smaller. The torque ripple when using the conventional DTC method is roughly 1.1 (N.m), but changes to 0.7 (N.m) with the proposed method.

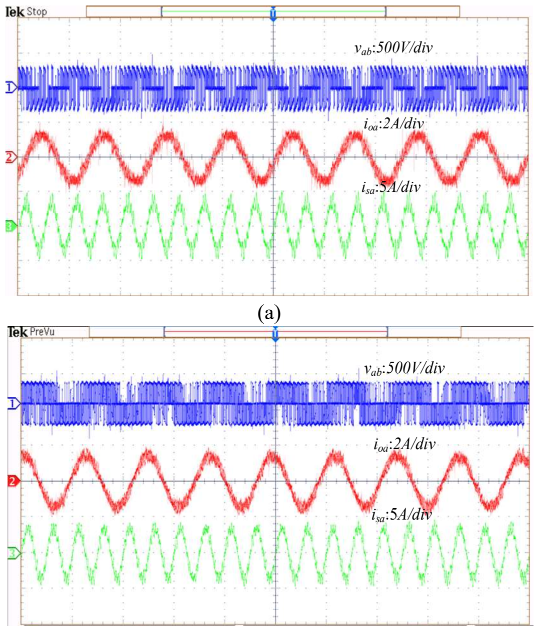

Fig. 7. Input and output waveforms of DMC with load torque equal to 0 (N.m) (a) under conventional DTC method [10ms/div] (b) under the proposed MPC-based DTC method [10ms/div]

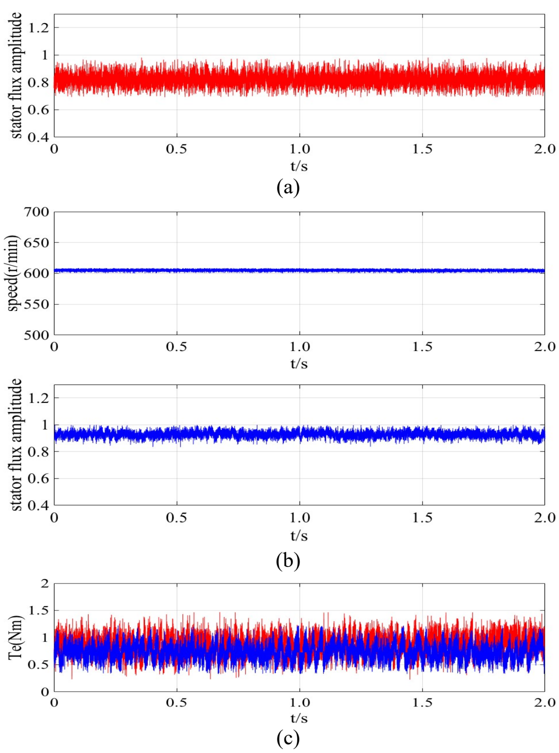

Fig. 8. Mechanical performance of IM with load torque equal to 0 (N.m) (a) Rotor speed and stator flux amplitude under conventional DTC method (b) Rotor speed and stator flux amplitude under the proposed MPC-based DTC method (c) Comparison of electromagnetic torque (Red: the proposed MPC-based DTC method, Blue: the conventional DTC method)

Fig. 9a and Fig.9b show the rotor speed and stator flux amplitude with the conventional DTC method and the proposed method. The reference speed is 600 (r/min), and the reference stator flux is 0.9 (Wb). The load torque of the IM is 2.5 (N.m) approximately. Fig. 9a represents the rotor speed and stator flux amplitude under the conventional DTC method and Fig. 9b represents the rotor speed and stator flux amplitude under the proposed method. As shown in these figures, both methods have similar effects on speed tracking and flux tracking.

Fig. 9c compares the electromagnetic torque by means of conventional DTC and the proposed MPC-based DTC method with the load torque equal to 2.5 (N.m), as shown in Fig. 9c. Both methods track load torque accurately, but the torque ripple using the proposed method is smaller. There is only 1.3(N.m) torque ripple under the MPC-based DTC method, but nearly 2(N.m) torque ripple under the conventional method.

Fig. 10 illustrates the waveform of the output line-to-line voltage, output current and grid current by means of the conventional DTC method and the MPC-based method under the same condition of that in Fig. 9. As for Fig.10, it shows that both methods have the ability to make grid current and output current sinusoidal with small distortion.

Fig. 11 illustrates the experimental results of the proposed method when the load torque changes suddenly. The proposed MPC-based DTC method inherits the advantage of the FCS-

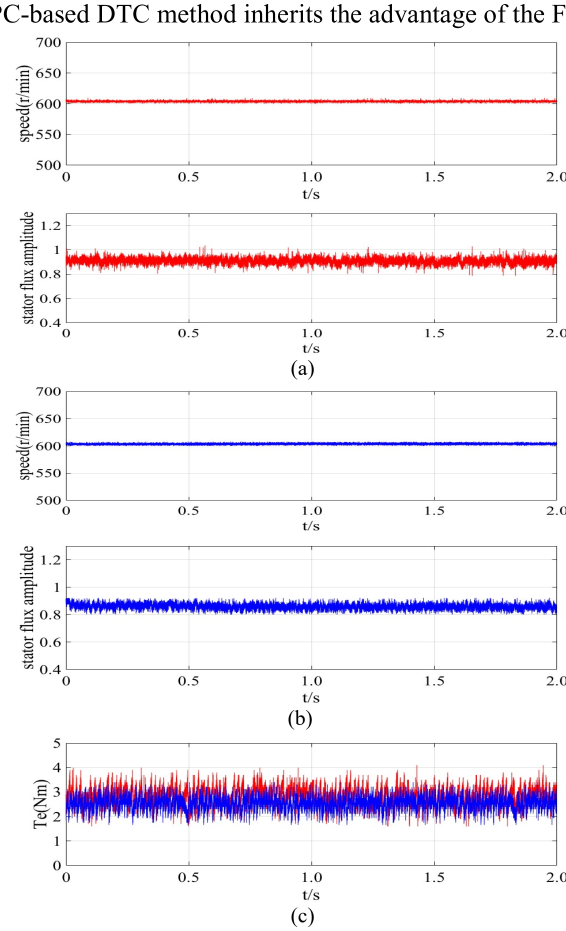

Fig. 9. Mechanical performance of IM with load torque equal to 2.5 (N.m) (a) Rotor speed and stator flux amplitude under conventional DTC method (b) Rotor speed and stator flux amplitude under the proposed MPC-based DTC

method (c) Comparison of electromagnetic torque (Red: the proposed MPC-based DTC method, Blue: the conventional DTC method)

MPC method, such as quick dynamic response, which can be seen in Fig. 11. The electromagnetic torque responds quickly when load torque changes and remains steady with no more than 0.5 seconds, the rotor speed drops a little because of the rapid change of load torque, but also remains steady with no more than 0.5 seconds.

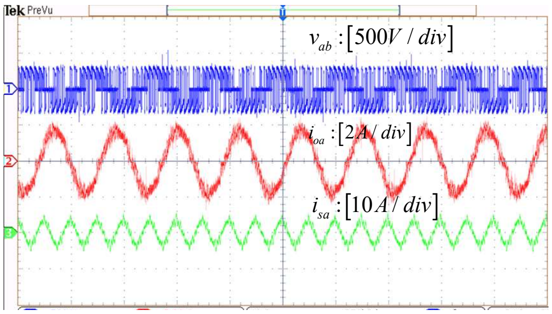

(a)

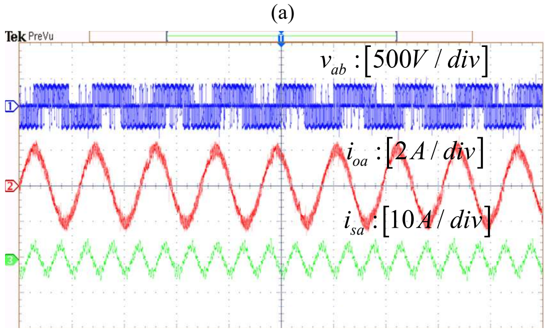

(b)

Fig. 10. Input and output waveforms of DMC with load torque equal to 2.5 (N.m) (a) Under conventional DTC method [10ms/div] (b) Under the proposed MPC-based DTC method [10ms/div]

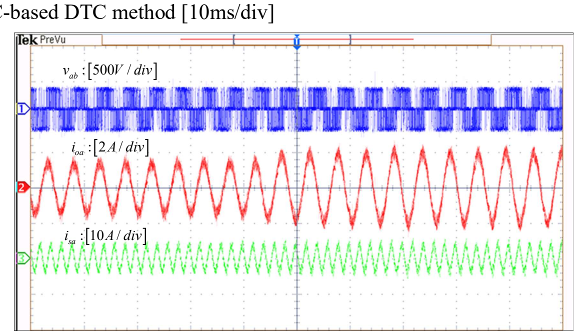

(a)

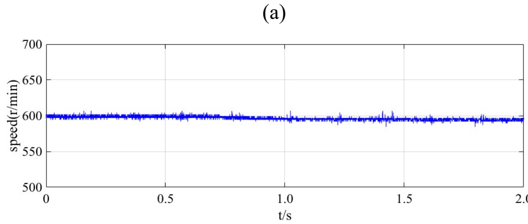

(b)

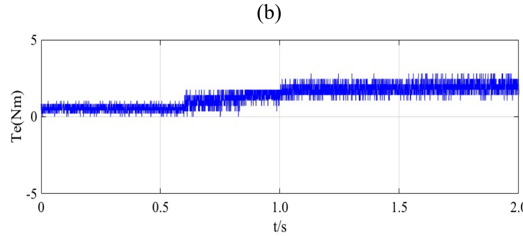

(c)

Fig. 11. Experimental results of the proposed MPC-based DTC method when the load torque changes suddenly (a) Input and output waveforms of DMC [10ms/div] (b) Rotor speed of IM (c) Electromagnetic torque of IM

VI. Conclusions

An MPC-based DTC method for a DMC-fed IM is presented in this paper. Six voltage vectors selected from two look-up tables along with three zero voltage vectors are utilized for prediction. The switching state which minimizes the cost function is selected as the optimal switching state for the next switching period. Compared with conventional DTC, the method in this paper not only considers the unused voltage vectors but also manages to achieve a similar control effect with the reduced torque ripple. Finally, experimental results have been presented to demonstrate and validate the effectiveness and correctness of the proposed MPC-based DTC method.

VII. Discussions

The electromagnetic torque ripple of the proposed MPC-based DTC method is less than that of the conventional DTC method under the same experimental condition. Compared with the conventional FCS-MPC method which evaluates 27 switching states, nine switching states are preselected and used to select the optimal switching state in the proposed MPC-based DTC method. Thus, the calculation effort of the proposed MPC-based DTC method is reduced compared with the conventional FCS-MPC method. The performance of the proposed MPC-based DTC strategy is nearly the same as the conventional FCS-MPC. This advantage will make the higher predictive horizon possible or implement the total algorithm on a cheaper microcontroller. This advantage is an expansion of the idea in [28]. The comparison among the conventional DTC method, conventional FCS-MPC method and proposed MPC-based DTC method is shown in Table VII. More number of signs "+" represent better performance in Table VII.

TABLE VII
Experimental Parameters

Parameters	Conventional DTC method	Conventional FCS-MPC method	MPC-based DTC method
Speed tracking	+++	+++	+++
Torque ripple	++	+++	+++
Calculation effort	+	+++	++

References

[1] P. W. Wheeler, J. Rodriguez, J. C. Clare, L. Empringham, and A. Wein-stein, "Matrix converters: A technology review," *IEEE Trans. Ind. Electron*., vol. 49, no. 2, pp. 276–288, Apr. 2002.

[2] J. Rodriguez, M. Rivera, J. W. Kolar, and P. W. Wheeler.: "A review of control and modulation methods for matrix converters," *IEEE Trans. Ind. Electron.*, vol. 59, no. 1, pp. 58–70, Jan. 2012.

[3] E. Yamamoto et al, "Development of MCs and its applications in industry," *IEEE Trans. Ind. Electron*., vol. 5, no. 1, pp. 4–12, Mar. 2011.

[4] Mohamed Basri Hazrul, Mekhilef Saad, "Experimental evaluation of model predictive current control for a modified three-level four-leg indirect matrix converter,". *IET Electric Power Applications*, 2017, 12 (1).

[5] P. Yao and X. Jiang, "An optimal six vector switching pattern in matrix converters for reducing harmonics and switching loss," in CSEE Journal

of Power and Energy Systems, doi: 10.17775/CSEEJPES.2019.03290.

[6] W. Deng, "Maximum Voltage Transfer Ratio of Matrix Converter under DTC with Rotating Vectors," in IEEE Transactions on Power Electronics, doi: 10.1109/TPEL.2020.3033414.

[7] D. Casadei, G. Serra, A. Tani, “The use of matrix converters in direct torque control of induction machines,” *IEEE Trans. Ind. Electron.*, vol. 4, pp. 1057-1064, 2001.

[8] Hong-Hee Lee, H. M. Nguyen, Tae-Won Chun and Won-Ho Choi, “Implementation of direct torque control method using matrix converter fed induction motor,” 2007 *International Forum on Strategic Technology, Ulaanbaatar*, pp. 51-55, 2007.

[9] R. H. Kumar, A. Iqbal and N. C. Lenin, “Review of recent advancements of direct torque control in induction motor drives – a decade of progress,” *IET Power Electronics*, vol. 11, no. 1, pp. 1-15, 12 1 2018.

[10] K. Lee and F. Blaabjerg, “Sensorless DTC-SVM for Induction Motor Driven by a Matrix Converter Using a Parameter Estimation Strategy,” *IEEE Transactions on Industrial Electronics*, vol. 55, no. 2, pp. 512-521, Feb. 2008.

[11] S. Sebtahmadi, H. Pirasteh, S. Kaboli, et al, “A 12-Sector Space Vector Switching Scheme for Performance Improvement of Matrix-Converter-Based DTC of IM Drive,” *IEEE Trans. Power Electron*, vol. 7, pp. 3804-3817, 2015.

[12] P. Cortes, M. P. Kazmierkowski, R. M. Kennel, D. E. Quevedo, and J. Rodriguez, “Predictive control in power electronics and drives,” *IEEE Trans. Ind. Electron*., vol. 55, no. 12, pp. 4312–4324, Dec. 2008.

[13] J. Rodriguez et al, “State of the art of finite control set model predictive control in power electronics,” *IEEE Trans. Ind. Informat.*, vol. 9, no. 2, pp. 1003–1016, May 2013.

[14] Sergio Vazquez, Jose I. Leon, Leopoldo G. Franquelo, Jose Rodriguez, et al., “Model Predictive Control: A Review of Its Applications in Power Electronics,” *IEEE Industrial Electronics Magazine*, vol. 8, no. 1, pp. 16-31, March 2014.

[15] M. Khosravi, M. Amirbande, D. A. Khaburi, M. Rivera, J. Riveros,J. Rodriguez, A. Vahedi, and P. Wheeler, "Review of model predictive control strategies for matrix converters," *IET Power Electronics*, vol. 12, no. 12, pp. 3021- 3032, 2019.

[16] A. Dekka, B. Wu, V. Yaramasu, R. L. Fuentes and N. R. Zargari, “Model Predictive Control of High-Power Modular Multilevel Converters—An Overview,” *IEEE Journal of Emerging and Selected Topics in Power Electronics.*, vol. 7, no. 1, pp. 168-183, March 2019.

[17] Y. Zhang, H. Yang and B. Xia, "Model predictive torque control of induction motor drives with reduced torque ripple," *IET Electric Power Applications*, vol. 9, no. 9, pp. 595-604, November 2015.

[18] Muslem Uddin, Saad Mekhilef, Marizan Mubin, Marco Rivera, Jose Rodriguez. “Model Predictive Torque Ripple Reduction with Weighting Factor Optimization Fed by an Indirect Matrix Converter,” *Electric Power Components and Systems*,vol. 42， no. 10, pp. 1059–1069, 2014.

[19] R. Vargas, J. Rodriguez, U. Ammann, and P. Wheeler, “Predictive current control of an induction machine fed by a matrix converter with reactive power control,” *IEEE Trans. Ind. Electron*., vol. 55, no. 12, pp. 4362–4371, Dec. 2008.

[20] R. Vargas, U. Ammann, B. Hudoffsky, J. Rodriguez, and P. Wheeler, “Predictive torque control of an induction machine fed by a matrix converter with reactive input power control,” *IEEE Trans. Power Electron.*, vol. 25, no. 6, pp. 1426–1438, Jun. 2010.

[21] Mohsen Siami, Davood Arab Khaburi, Marco Rivera, Jose Rodríguez, “A Computationally Efficient Lookup Table Based FCS-MPC for PMSM Drives Fed by Matrix Converters,” *IEEE Trans. Ind. Electron*., vol. 64, no. 10, pp. 7645-7654, Oct. 2017.

[22] M. Siami, D. Arab Khaburi and J. Rodriguez, “Simplified Finite Control Set-Model Predictive Control for Matrix Converter-Fed PMSM Drives,” *IEEE Transactions on Power Electronics*, vol. 33, no. 3, pp. 2438-2446, March 2018.

[23] T. Peng, M. Wen, Z. Li, Z. Xu, J. Yang, “An improved DTC strategy for induction motors fed by direct matrix converter,” in *Proc. of 2015 Chinese Automation Congress*. IEEE, 2015: 1766-1771.

[24] P. Cortes, S. Kouro, B. La Rocca, R. Vargas, J. Rodriguez, J. I. Leon, S. Vazquez, and L. G. Franquelo, “Guidelines for weighting factors design in Model Predictive Control of power converters and drives,” in *Proc. of IEEE ICIT*, pp. 1 - 7, 2009.

[25] T. Dragicevic and M. Novak, “Weighting Factor Design in Model Predictive Control of Power Electronic Converters: An Artificial Neural Network Approach,” *IEEE Transactions on Industrial Electronics*, vol. 66, no. 11, pp. 8870 - 8880, 2019.

[26] P. L. Jansen et al, “A Physically Insightful Approach to the Design and Accuracy Assessment of Flux Observers for Field Oriented Induction Machine Drives,” *IEEE Trans. Ind. Appl*., vol. 38, pp. 1334-1343, Sep./Oct. 2002.

[27] Jang-Hwan Kim, Jong-Woo Choi and Seung-Ki Sul, “Novel rotor-flux observer using observer characteristic function in complex vector space for field-oriented induction motor drives,” *IEEE Transactions on Industry Applications*, vol. 38, no. 5, pp. 1334-1343, Sept.-Oct. 2002.

[28] H. Dan, Q. Zhu, T. Peng, Y. Sun, P. Wheeler, “Preselection algorithm based on predictive control for direct matrix converter,” *IET Electric Power Applications*, vol. 11, pp. 768-775, May 2017.

Hanbing Dan was born in Hubei, China, in 1991. He received the B.S. degree in Automation, and Ph.D. degree in Control Science and Engineering from Central South University, Changsha, China, in 2012, and 2017, respectively. He was a visiting researcher in Faculty of Engineering at the University of Nottingham, United Kingdom during 2017. He is currently an associate professor with the School of Automation, Central South University, China.

His research interests include power converter, motor control, model predictive control, fault diagnosis.

Peng Zeng was born in Jiangxi, China, in 1996. He received the B.S. degree in electrical engineering and the automatization from Jiangsu University, China, in 2019. He is currently studying for a master's degree in electrical engineering at Central South University.

His research interests include power converter, motor control, model predictive control, fault diagnosis.

Wenjing Xiong was born in Hunan, China, in 1991.She received the B.S. degree in Automation, and Ph.D degree in Control Science and Engineering from Central South University, Changsha, China, in 2012, and 2017, respectively. She is currently an associate professor with the School of Automation, Central South University, China.

Her research interests include modulation strategy for power converters, matrix converter, ac/dc converter and wireless power transfer.

Meng Wen was born in Shandong, China, in 1990. She received the B.S. degree in Automation from Kunming University of Science and Technology, Kunming, China, in 2013. She received master degree in Control Science and Engineering from Central South University, Changsha, China, in 2016. She is currently an engineer in Yunnan Mobile Communication Company Limited.

Mei Su (Member, IEEE) was born in Hunan, China, 1967. She received the B.S. degree in automation, the M.S. degree in automation, and the Ph.D. degree in control science and engineering from Central South University, Changsha, China, in 1989, 1992, and 2005, respectively. She has been a Full Professor with the School of Automation, Central South University. She is currently an Associate Editor of the IEEE Transactions on Power Electronics.

Her research interests include matrix converter, adjustable speed drives, and wind energy conversion system.

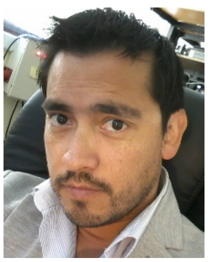

Marco Rivera (Senior Member, IEEE) received his B.Sc. in Electronics Engineering and M.Sc. in Electrical Engineering from the Universidad de Concepcion, Chile, in 2007 and 2008, respectively. He received his PhD degree from the Department of Electronics Engineering, Universidad Tecnica Federico Santa Maria, in Valparaiso, Chile, in 2011 with a scholarship from the Chilean Research Fund CONICYT. During 2011 and 2012, Prof. Rivera held a Post Doctoral position and worked as part-time professor of Digital Signal Processors and Industrial Electronics at Universidad Tecnica Federico Santa Maria. Currently he is an Associate Professor in the Faculty of Engineering at Universidad de Talca, Curico, Chile. Prof. Rivera Abarca was awarded a scholarship from the Marie Curie Host Fellowships for early stage research training in electrical energy conversion and conditioning technology at the University College Cork, Cork, Ireland in 2008. In 2012, Prof. Rivera was awarded the Chilean Academy of Science Doctoral Thesis Award (Premio Tesis de Doctorado Academia Chilena de Ciencias), for the best PhD thesis published in 2011, selected from among all national and international students enrolled in any exact or natural sciences program in Chile and he was awarded as an Outstanding Engineer in 2015.

He is the Head of the Laboratory of Energy Conversion and Power Electronics (LCEEP) and the Technology Center for Energy Conversion (CTCE). His research interests include matrix converters, predictive and digital controls for high-power drives, four-leg converters, renewable energies and development of high-performance control platforms based on Field- Programmable Gate Arrays.